Laser Flash Absorption Spectroscopy Study of Ferredoxin Reduction by Photosystem I: Spectral and Kinetic Evidence for the Existence of Several Photosystem I−Ferredoxin Complexes

Pierre Q. Y. Sétif* and Hervé Bottin

Département de Biologie Cellulaire et Moléculaire, Section de Bioénergétique, CEA, and CNRS URA 1290, CE Saclay, 91191 Gif sur Yvette, France

Received March 2, 1995[⊗]

ABSTRACT: The existence of three first-order phases has been previously reported for the reduction of soluble ferredoxin by photosystem I (PSI), both from the cyanobacterium *Synechocystis* sp. PCC 6803 (at pH 8 and in the presence of salts) [Sétif, P. Q. Y., & Bottin, H. (1994) *Biochemistry 33*, 8495−8504]. The spectra of these three phases ($t_{1/2}$ < 1 μs, = 13−20 and 103−123 μs) have been measured between 460 and 600 nm. All of them are fully consistent with electron transfer from $(F_A,F_B)^-$, the terminal 4Fe-4S acceptors of PSI, to ferredoxin. Though the three spectra deviate significantly from the spectrum that can be calculated independently for this process, their sum closely matches the calculated spectrum. A detailed examination of these deviations indicates that the intermediate (13−20 μs) and slow (103−123 μs) first-order phases are associated with two distinct ferredoxin-binding sites on PSI. Under the same conditions, a fourth phase of negative amplitude is also observed in the 460−600 nm region. It is ascribed to reoxidation of reduced ferredoxin by an unknown species. The kinetic properties of this process show that it is triggered by collision of free ferredoxin with a preformed PSI−ferredoxin complex. Taking this reaction into account, it is shown that the relative proportions of the three first-order phases of ferredoxin reduction do not depend upon the ferredoxin concentration, indicating that the different sites of ferredoxin binding are mutually exclusive. The kinetics of ferredoxin reduction were also studied at pH 5.8, in the absence of salts. Under these conditions, the affinity of ferredoxin for PSI is much higher than at pH 8 (dissociation constant ≈ 0.05 μM versus 0.6 μM) and the kinetics of ferredoxin reduction are much faster (a major submicrosecond phase and a single first-order microsecond phase with $t_{1/2}$ ≈ 9 μs), whereas a third, slower first-order phase is essentially absent. Two similar first-order components are found for the reduction of spinach ferredoxin by PSI from *Synechocystis* at pH 8, though the apparent dissociation constant for the latter system is larger (≈5 μM). Despite the different affinities of spinach and *Synechocystis* ferredoxins for the cyanobacterial PSI, similar second-order rate constants are found in both cases at pH 8 [(2−6) × 10^8 M^{-1} s^{-1}].

Photosystem I (PSI)[1] is a light-driven transmembrane oxidoreductase found in oxygenic photosynthetic organisms. It oxidizes plastocyanin on the lumenal side of the photosynthetic membrane and reduces ferredoxin on the stromal side. In some cyanobacteria and algae, plastocyanin and ferredoxin can be replaced by cytochrome c_6 and flavodoxin, respectively (Ho & Krogmann, 1984; Rogers, 1987). The PSI reaction center is a large complex (ca. 300 kDa) containing at least 11 (in cyanobacteria) or 13 (in chloroplasts) different subunits and about 90−100 chlorophyll molecules (Golbeck & Bryant, 1991). It is embedded in the photosynthetic membrane but also contains several protruding peripheral subunits. Two of these peripheral subunits, PSI-D and PSI-E, have been found to play some role in the interaction of PSI with soluble ferredoxin (Zanetti & Merati, 1987; Zilber & Malkin, 1988; Andersen et al., 1992a,b; Sonoike et al., 1993; Rousseau et al., 1993; Lelong et al., 1994). Reduction of soluble ferredoxin by PSI is preceded by a multistep charge separation within the reaction center. This charge separation involves first the photochemical formation of the oxidized primary donor $P700^+$ (a dimer of chlorophyll molecules) and the reduced primary acceptor A_0 (a chlorophyll molecule), leading eventually to the reduction of one or both of the terminal acceptors F_A and F_B. These two acceptors are 4Fe-4S centers which are both carried by a small subunit named PSI-C, which is firmly associated to the core of the PSI reaction center. This core is mainly composed of the two large and closely related membrane-spanning subunits, PSI-A and PSI-B, which carry the antenna chlorophylls, most of the carotenoids, and the electron-transferring cofactors P700, A_0 and the secondary acceptors A_1 (a phylloquinone molecule) and F_X (a 4Fe-4S center) (Golbeck & Bryant, 1991).

The direct observation of ferredoxin reduction by isolated PSI was made only recently by laser flash absorption spectroscopy (Hervas et al., 1992; Rousseau et al., 1993; Sétif & Bottin, 1994). In a recent study conducted mostly with PSI and ferredoxin from the cyanobacterium *Synechocystis* sp. PCC 6803, three different first-order phases of ferredoxin reduction by PSI were found (at pH 8 and at moderate ionic strength) with half times of ca. 500 ns, 20 μs, and 100 μs (Sétif & Bottin, 1994). It was assumed that all three phases

⊗ Abstract published in *Advance ACS Abstracts,* June 15, 1995.

[1] Abbreviations: PSI, photosystem I; F_A, F_B, and F_X, the 4Fe-4S centers of photosystem I; Fd, ferredoxin; β-DM, *n*-dodecyl β-D-maltoside; DPIP, (2,6-dichlorophenol)indophenol; MES, 2-(*N*-morpholino)ethanesulfonic acid; K_d, dissociation constant; Δ*A*, flash-induced absorption change.

0006-2960/95/0434-9059$09.00/0

were resulting from electron transfer in PSI−ferredoxin complexes that were preformed before flash excitation and that the immediate partner of ferredoxin is either F_A or F_B. It was also suggested that at least two different types of PSI−ferredoxin complexes must coexist in order to explain the above kinetic complexity. In the following, we characterize further the kinetics of electron transfer between PSI and ferredoxin in different systems and we describe the spectral features of the different kinetic components.

MATERIALS AND METHODS

Biological Samples. Most of the studies described here were made with monomeric PSI reaction centers from *Synechocystis* 6803 (Rögner et al., 1990; Kruip et al., 1993). The same batch of monomeric PSI reaction centers was used throughout this study. The membranes were solubilized with 1% (w/v) *n*-dodecyl β-D-maltoside (β-DM), and purification was stopped after the centrifugation step on a sucrose density gradient. The PSI reaction centers were dialyzed against 20 mM tricine/NaOH, pH 7.5, and 0.03% β-DM and concentrated by ultrafiltration (Centriprep 100, Amicon). Chlorophyll concentration was determined according to Arnon (1949). The P700 content was calculated from photoinduced absorption changes at 820 nm assuming an absorption coefficient of 6500 M^{-1} cm^{-1} for $P700^+$ (Mathis & Sétif, 1981). The chlorophyll to P700 ratio was found to be 90 ± 5 in isolated monomeric PSI reaction centers. D144 particles from spinach were prepared according to Boardman (1971). The chlorophyll to P700 ratio in these particles was found to be 220 ± 20.

Ferredoxin from *Synechocystis* was prepared according to Bottin and Lagoutte (1992). The oxidized minus reduced difference spectrum of ferredoxin was measured in 33 mM Tris-HCl, pH 8.5. Ferredoxin was reduced by 5 mM sodium dithionite in the absence of redox mediators. Under these conditions, the ambient redox potential is below −500 mV. Assuming a value of −412 mV for the midpoint potential of ferredoxin (Bottin & Lagoutte, 1992), more than 97% of the ferredoxin should be reduced under these conditions. An absorption coefficient of 9500 M^{-1} cm^{-1} for oxidized ferredoxin at 423 nm (relative maximum) (Tagawa & Arnon, 1968; Fee & Palmer, 1971) was assumed for calculating the differential absorption coefficients. The maximum of the difference spectrum was found at 428.5 nm ($\Delta\epsilon = 5000 \pm 100$ M^{-1} cm^{-1}). Ferredoxin from spinach was provided by Dr. J.-P. Jacquot.

Flash Absorption Spectroscopy and Calculation of Composite Kinetic Curves. Measurements were made at 296 K as described previously with a microsecond time resolution (Sétif & Bottin, 1994). Except when indicated, square cuvettes (1 × 1 cm) were used. An average of 16−64 experiments was made for each kinetic curve with a repetition rate of 0.1 Hz for laser flash excitation. The measuring wavelength was selected with two interference filters placed before and after the cuvette. The band width resulting from the combined use of these two filters was found to lie between 5 and 10 nm. For calculating the absorption changes corresponding to electron transfer from ferredoxin to (F_A,F_B), the difference spectrum of ferredoxin (obtained with a band width of 2 nm) was convoluted with the transmission curve of the two interference filters used for flash absorption spectroscopy. In a previous study (Sétif & Bottin, 1994), differences between flash-induced absorption changes measured in the presence and absence of ferredoxin [$\Delta(\Delta A)$] were shown for some experiments. Such a procedure was justified by the fact that, in the absence of ferredoxin, there was no significant transient signal following the flash during the time under study (≤1 ms after flash excitation), except for some antenna components which are eliminated through the subtraction procedure (Sétif & Bottin, 1994). This absence of transient signal is due to the fact that, on the time scale under study and without added ferredoxin, the decay of both $P700^+$ and $(F_A,F_B)^-$ is negligible. Under these approximations, the $\Delta(\Delta A)$'s were directly interpreted as resulting from electron transfer between PSI acceptors, including ferredoxin, in the presence of the latter. However the subtraction procedure becomes no longer valid for longer times after flash excitation, as the recombination of $P700^+$ with $(F_A,F_B)^-$ in the absence of ferredoxin cannot be neglected, especially at wavelengths where the signals due to ferredoxin reduction are rather small, e.g., above 560 nm and at 460 nm. It was also found that the subtraction procedure gives poor results for the study of spinach particles, even on a 1 ms time scale. This is due to the fact that the recombination reaction between $P700^+$ and $(F_A,F_B)^-$ is significantly faster in spinach particles than in cyanobacterial PSI ($t_{1/2} \approx 30$ ms versus 100 ms; not shown). Under such conditions, the decay of $P700^+$ cannot be neglected, even on a 1 ms time scale.

For the above reasons, another procedure was devised for displaying the absorption changes due to electron transfer in the presence of ferredoxin for times as long as several 10's of milliseconds (Figure 1). The following conditions must be fulfilled for an appropriate treatment of the data: (a) the contribution due to $P700^+$ decay should be eliminated together with (b) the contribution of antenna triplet states; (c) in experiments recorded with a microsecond time resolution, the initial signal size after the flash should be obtained for having an estimate of an eventual unresolved submicrosecond component; and (d) in the final kinetic curve, the decay of $(F_A,F_B)^-$ which is occurring in the absence of ferredoxin should of course not be taken into account. The different steps of this procedure are described in the following for a given wavelength, λ, between 460 and 600 nm. (1) After recording the kinetic transients without or with ferredoxin (traces 1a and 2a), the contribution of $P700^+$ decay (traces − and +) was first subtracted from both curves (traces 1b and 2b), knowing the differential absorption coefficients of ($P700^+$ − P700) at λ and at 820 nm (condition a). (2) The kinetics recorded in the absence of ferredoxin were subtracted from those observed in its presence (trace 3). This allows to eliminate the contribution due to antenna triplet states (condition b) and to get the initial amplitude of the signal in the presence of ferredoxin (condition c). However the contribution due to $(F_A,F_B)^-$ decay in the absence of ferredoxin has also been subtracted during this step. As long as this decay is negligible ($t < t_1$), trace 3 depicts reliably the absorption changes of interest. However, for longer times ($t > t_1$), the electron transfer process in the presence of ferredoxin is truly monitored by trace 2b. (3) For getting reliable kinetics of absorption changes due to PSI acceptors (including ferredoxin) in the presence of ferredoxin at any time after flash excitation, a composite curve was built from traces 3 (valid for $t < t_1$) and 2b (valid for $t > t_1$). This was

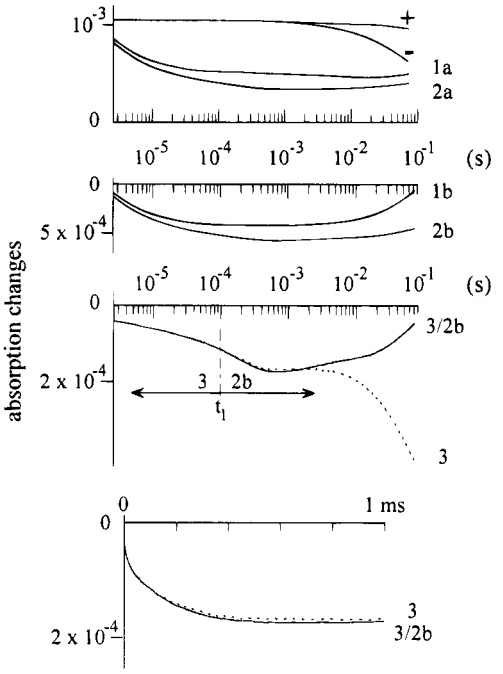

FIGURE 1: Different steps involved in the procedure for displaying the absorption changes due to electron transfer between PSI acceptors, including ferredoxin, in the presence of the latter. With the exception of the lower curves, a logarithmic time scale is used allowing to exhibit the absorption changes from 2 μs to 72 ms after flash excitation. For the sake of clarity, the traces that are shown are simulated curves obtained at 480 and 820 nm after fitting experimental data. The conditions of the corresponding experiment are the following: 0.173 μM PSI, 0.99 μM ferredoxin (when added), 20 mM tricine, pH 8, 30 mM NaCl, and 5 mM $MgCl_2$. In the absence of ferredoxin, traces 1a and − are obtained at 480 and 820 nm, respectively. In the presence of ferredoxin, traces 2a and + are obtained at these two wavelengths. Traces 1b and 2b are obtained after subtracting the contributions of $P700^+$ decay (as recorded by traces − and +) from traces 1a and 2a. This was done after measuring the relative absorption coefficients of ($P700^+$ − P700) at 480 and 820 nm. Trace 3 corresponds to the difference between traces 2b and 1b. Trace 3/2b is a composite curve identical to trace 3 for times < t_1 (t_1 = 100 μs) and identical to trace 2b for times > t_1, after adding to trace 2b an offset such that there is continuity at time t_1. Expanded portions of traces 3 and 3/2b are displayed at the bottom on a linear time scale.

done by adding an offset to trace 2b so that the resulting curve is continuous at time t_1 (trace 3/2b).

The value of time t_1, as defined above, can be generally chosen between values of 80 μs and 1 ms: before 80 μs, the antenna triplet states have not fully decayed, and after 1 ms (in some cases after a few 100's of microseconds), the $(F_A,F_B)^-$ decay in the absence of ferredoxin cannot be completely neglected. For the data shown in the present study, t_1 = 80−120 μs.

Data were fitted with several exponential components using a Marquardt algorithm. A global fit procedure was used (Beechem, 1992) either for obtaining spectra in the 460−600 nm region or for fitting a series of kinetic curves obtained at different ferredoxin concentrations and exhibiting phases with identical half times.

Decay-Associated Spectra Associated with Different PSI−Ferredoxin Complexes. For the analysis of the absorption changes observed at pH 8 with PSI and ferredoxin from *Synechocystis*, we consider in the following three different types (I, II, and III) of PSI−ferredoxin complexes which are exclusive one from the other. For each of these complexes, the spectra of F_A,F_B and ferredoxin are considered to be potentially different as compared to their free forms. We will consider in the following calculations only the PSI reaction centers that form one complex or another with ferredoxin and will not take into account P700, the contribution of which is eliminated by the calculation of composite curves (see the preceding paragraph). Complexes I, II, and III [amounts (1 − α − β), α, and β] are considered to correspond to the fastest, intermediate, and slowest first-order components observed at pH 8.

For example, the absorption contribution of complex I is $(1 - \alpha - \beta)OD(\lambda)_{(F_A,F_B)_IFd_I}$ or, in simplified form, $(1 - \alpha - \beta)FAB_IFd_I$ before the flash excitation. After completion of the fast phase, this contribution becomes $(1 - \alpha - \beta)FAB_IFd_I^-$.

In the absence of ferredoxin (reference sample), the absorption of PSI is FAB before the flash excitation. It becomes $(FAB)^-$ at the time which corresponds to completion of the fast phase when ferredoxin is present, assuming that F_A,F_B is reduced within a few 100's of nanoseconds (Sétif & Bottin, 1994). It is observed that this absorption remains unchanged on a time scale of several 100's of microseconds. At later times after flash excitation, the further absorption changes due to decay of $(F_A,F_B)^-$ in the absence of ferredoxin are of no matter when considering composite kinetic traces (see above). The spectra U_I and V_I are defined as follows:

$$U_I = (FAB_I^- - FAB_I) - (FAB^- - FAB) \text{ and } V_I = (Fd_I^- - Fd_I) - (Fd^- - Fd)$$

U_I corresponds to the difference between the differential spectra of F_A,F_B observed within complex I and in the absence of complex. V_I is the same quantity evaluated for ferredoxin. In the same manner, U_{II}, V_{II}, U_{III}, and V_{III} can be defined for complexes II and III. The spectrum that can be calculated for electron transfer from $(F_A,F_B)^-$ to ferredoxin from the independent measurement of the two spectra due to F_A,F_B and ferredoxin reduction (both obtained in the absence of complex) is

$$C = (Fd^- - Fd) - (FAB^- - FAB)$$

The spectra of the three different phases and of their sum can be easily calculated from the above quantities:

fast phase (as obtained from subtracting the signal recorded in the absence of ferredoxin from that recorded in its presence) = $(1 - \alpha - \beta)(C + V_I) + \alpha U_{II} + \beta U_{III}$

intermediate phase = $\alpha(C + V_{II} - U_{II})$

slow phase = $\beta(C + V_{III} - U_{III})$

sum of three phases = $C + (1 - \alpha - \beta)V_I + \alpha V_{II} + \beta V_{III}$

It should be noted here that a bleaching accompanying ferredoxin reduction will be shown in the Results section as a positive amplitude, as an absorption decrease corresponds to a positive amplitude of the decay-associated spectrum. The above simple relations will be used in order to compare

the decay-associated spectra of the three first-order phases observed at pH 8. It is interesting to note that when considering the sum of the three phases, deviation from the calculated spectrum C should arise only from distortion of the differential spectra of ferredoxin when bound to PSI. These results can still be applied to all three phases in the case where two of them correspond to only one type of PSI–ferredoxin complex, as long as every decay-associated spectrum corresponds to a redox transition between two well-defined redox states.

Dissociation Constants of Mutually Exclusive PSI–Ferredoxin Complexes. We consider here n different PSI–ferredoxin complexes which are exclusive one from the other, assuming a simple binding equilibrium for each of these complexes:

$$PSI + Fd \rightleftarrows [PSI{\cdot}FD]_i$$

with dissociation constant

$$K_{d_i} = [PSI][Fd]/[PSI{\cdot}Fd]_i \quad (1)$$

From (1), one can derive

$$[PSI{\cdot}Fd]_i/(1/K_{d_i}) = [PSI{\cdot}Fd]_j/(1/K_{d_j}) = [PSI_{complex}]/K \quad (2)$$

with

$$[PSI_{complex}] = \sum_{(i=1..n)} [PSI{\cdot}Fd]_i \text{ and } K = 1/[\sum_{(i=1..n)} (1/K_{d_i})]$$

Combining (1) and (2) gives

$$K = [PSI][Fd]/[PSI_{complex}] \quad (3)$$

Equation 3 is equivalent to eq 1 by replacing K_{d_i} with K and $[PSI{\cdot}Fd]_i$ with $[PSI_{complex}]$, both equations turning out to be quadratic equations in $[PSI_{complex}]$ and $[PSI{\cdot}Fd]_i$, respectively, when knowing the total PSI and ferredoxin concentrations.

As a result, when analyzing the dependence of signal amplitude upon ferredoxin concentration (due to electron transfer within PSI–ferredoxin complexes preformed before the flash excitation), the apparent dissociation constant thus found is $K = 1/[\sum_{(i=1..n)}(1/K_{d_i})]$. The proportion of electron transfer associated with complex no. i is derived from eq 2:

$$[PSI{\cdot}Fd]_i/[PSI_{complex}] = K/K_{d_i}$$

which can be used to derive K_{d_i} when knowing this proportion and the dissociation constant K.

RESULTS

Spectral and Kinetic Characterization with PSI and Ferredoxin from Synechocystis 6803. In the first study of ferredoxin reduction by PSI from the cyanobacterium *Synechocystis*, we made use of the fact that 4Fe-4S and 2Fe-2S centers exhibit different absorption properties, the latter species exhibiting a more intense differential (oxidized minus reduced) spectrum than the former between 480 and 600 nm. Figure 2 shows such difference spectra from 460 to 600 nm for both the one-electron reduction of F_A,F_B (●) and soluble ferredoxin (+; see Materials and Methods). The spectrum of the difference $[F_A,F_B - (F_A,F_B)^-]$ was measured at pH 8 (30 mM NaCl, 5 mM $MgCl_2$) by comparing the absorption

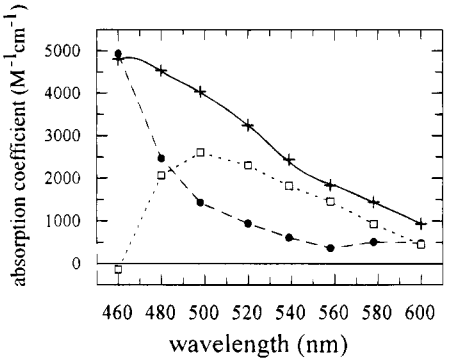

FIGURE 2: Oxidized minus reduced difference spectra of soluble ferredoxin (+; these values were calculated from the convolution of the continuous spectrum with the transmission spectra of the interference filters used for flash absorption spectroscopy; see Materials and Methods) and F_A,F_B (one-electron reduction; ●). The difference between the two spectra (□) corresponds to the spectrum which is expected for electron transfer from $(F_A,F_B)^-$ to ferredoxin.

changes in the absence and presence of 50 μM methylviologen on a 10 ms time scale (Ke, 1973; see Sétif and Bottin (1994), Figure 5, inset]. As already discussed (Sétif & Bottin, 1994), the spectrum of $[F_A,F_B - (F_A,F_B)^-]$ is larger in the 460–600 nm region than it was previously found [see, e.g., Ke (1973)] and than it is generally assumed. A differential absorption coefficient of 8000 ± 300 M^{-1} cm^{-1} was also found at 430 nm. The extinction coefficients of F_A,F_B were calculated by comparison to signals recorded at 820 nm on the same samples, assuming an absorption coefficient of 6500 M^{-1} cm^{-1} for $P700^+$ at this wavelength (Mathis & Sétif, 1981). Except at 460 nm, where the two species exhibit similar differential absorption coefficients, reduction of soluble ferredoxin corresponds to a larger bleaching than reduction of (F_A, F_B). Electron transfer from F_A,F_B to ferredoxin should therefore be accompanied by some absorption decrease above 460 nm. The decay-associated spectrum corresponding to such an electron transfer reaction can be calculated from the above spectra and is shown in Figure 2 (□).

The upper part of Figure 3 shows the flash-induced absorption changes at 480 nm due to ferredoxin addition under two different conditions: the left curve is obtained at pH 8 and in the presence of salts (30 mM NaCl, 5 mM $MgCl_2$), whereas the right curve is observed at pH 5.8 in the absence of salts. Both curves are composite curves (see Materials and Methods) which directly exhibit the kinetics of ferredoxin reduction by F_A,F_B. In the following, such composite curves will be generally shown, except when explicitly indicated. A fast submicrosecond phase is present in both kinetics shown in Figure 3, this phase being unresolved owing to the limited time resolution. This component was previously studied with a higher time resolution, and its half time is ca. 500 ns at pH 8 (Sétif & Bottin, 1994). It has not been further studied yet at pH 5.8 with such a higher time resolution and will be thereafter designated as the submicrosecond component. An absorption decrease in the microsecond range is also observed under both conditions. Fitting these components with one exponential phase gives satisfactory results at pH 5.8 ($t_{1/2} \approx 10$ μs) but not at pH 8, as can be seen from the corresponding residuals in Figure 3. It has been previously reported that, at pH 8, the microsecond decay is biphasic with two phases of 20 and 100 μs half times (Sétif & Bottin, 1994). It should

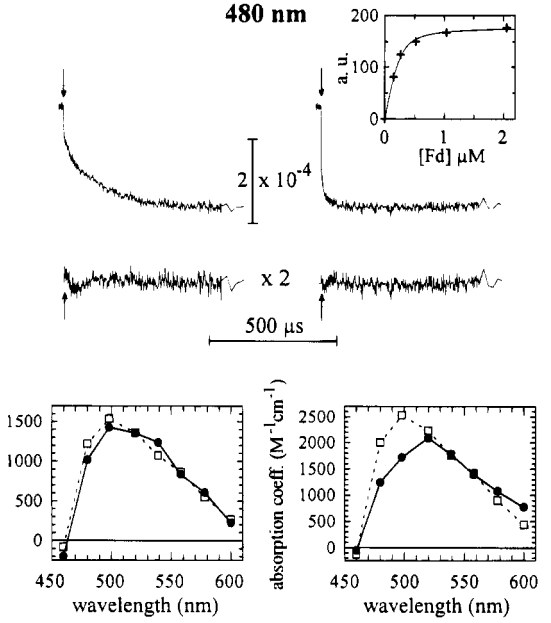

FIGURE 3: Upper part, composite curves exhibiting the kinetics of ferredoxin reduction by F_A,F_B. Left curve, 20 mM tricine, pH 8, 30 mM NaCl, 5 mM $MgCl_2$, 10 μM DPIP, 0.173 μM PSI, and 1.61 μM ferredoxin. Right curve, 20 mM MES, pH 5.8, in the absence of salts, 50 μM DPIP, 0.178 μM PSI, and 1.70 μM ferredoxin. In both cases, kinetics were recorded in the presence of 0.03% β-DM and 1.5 mM sodium ascorbate. Both curves were fitted with one exponential phase (halftimes of 94 and 10 μs at pH 8 and 5.8, respectively), and the corresponding residuals (multiplied by 2) are shown below the curves. Inset, the sum of the amplitudes of the two components found at pH 5.8 ($t_{1/2}$ < 1 μs and $\approx$ 10 μs) is plotted versus the ferredoxin concentration (0.178 μM PSI) and was fitted assuming a simple binding equilibrium between PSI and ferredoxin (apparent $K_d \approx 0.047$ μM). Lower part, the closed circles correspond to the sum of the decay-associated spectra of the first-order phases of ferredoxin reduction recorded at either pH 8 (left) or pH 5.8 (right). These spectra were obtained from a global fit of absorption changes measured between 460 and 600 nm on curves similar to those described above for 480 nm. The conditions were as defined above except for the PSI and ferredoxin concentrations at pH 8 (respectively 0.186 and 0.99 μM). The global analysis was conducted with two components at pH 8 and only one at pH 5.8. The result of this analysis gives half times of 13−20 and 103−123 μs at pH 8 (four different spectra of absorption changes were recorded with similar samples and analyzed independently; the indicated values correspond to the extreme values found for both components) and 9.0 μs at pH 5.8. An additional submicrosecond component is also present at both pH values. Its amplitude is taken as the initial value of the absorption change that is derived from the fitting procedure with microsecond phases. The sum of the amplitudes of the three (at pH 8) or two (at pH 5.8) components is plotted by reference to the signal measured at 820 nm for the same samples (ϵ = 6500 M^{-1} cm^{-1} for $P700^+$). For comparison, the expected spectrum for electron transfer from $(F_A,F_B)^-$ to ferredoxin is plotted in each case (□). This spectrum corresponds to the one shown in Figure 2 and is multiplied by the proportion of PSI forming a complex with soluble ferredoxin before flash excitation. This proportion is derived from fitting the dependence of signal amplitude on ferredoxin concentration by a simple binding equilibrium (inset for pH 5.8, apparent K_d = 0.047 μM; see below and Figure 10 for pH 8, apparent K_d = 0.62 μM). With the concentrations used for measuring these spectra, these proportions are 59% and 97% at pH 8 and 5.8, respectively.

be emphasized that, in trimeric PSI reaction centers from *Synechocystis* 6803, the same biphasic character is observed at pH 8 in the microsecond range. In the single batch of monomeric PSI used for the present study, half times were found to lie between 13 and 20 μs for the first microsecond component and between 103 and 123 μs for the second one (see legend of Figure 3). By contrast, the microsecond decay observed at pH 5.8 was found to be essentially monophasic at any wavelength studied from 460 to 600 nm. The half time of the microsecond component was found to be 9.0 ± 2 μs. It is independent of the measuring wavelength and the ferredoxin concentration. It is also observed that, from 480 to 600 nm, the amplitude of the submicrosecond component represents at least 40% of that of the total absorption decrease at pH 5.8. These different characteristics show that ferredoxin reduction is significantly faster at pH 5.8 than at pH 8. The dependence of the signal amplitudes on the ferredoxin concentration was studied at pH 5.8 and found to be identical for both phases ($t_{1/2}$ < 1 μs and $\approx$ 9 μs). The inset of Figure 3 (upper part) shows this dependence for the sum of the two phases recorded at 580 nm. The data were fitted assuming a simple binding equilibrium between PSI and ferredoxin, and an apparent dissociation constant of 47 nM was calculated. This value is about 10 times smaller than the dissociation constant observed at pH 8 [0.22−0.83 μM in Sétif & Bottin (1994) and 0.62 μM for the batch of monomeric PSI used throughout this study; see below]. Most of the above results concerning the kinetics of ferredoxin reduction are collected in Table 1. Figure 3 (bottom, ●) shows also the sum of the decay-associated spectra due to either the three components (at pH 8; left spectrum) or the two components (at pH 5.8; right spectrum) of absorption changes which are elicited by the addition of ferredoxin. The amplitudes of these spectra were calculated by reference to the signal of $P700^+$ at 820 nm (assuming ϵ = 6500 M^{-1} cm^{-1}). For comparison, the expected spectrum for electron transfer from $(F_A,F_B)^-$ to ferredoxin is plotted in each case (□) after multiplication by a factor which takes into account the proportion of PSI forming a complex with soluble ferredoxin before flash excitation (see legend of Figure 3 for details). This multiplication procedure is justified by the fact that the relative amplitudes of the three phases are not dependent upon ferredoxin concentration (see below and Figure 10). A fairly low value of ferredoxin concentration (0.99 μM) was preferred at pH 8 for a reliable spectral characterization, due to the presence of another phase of significant amplitude at higher ferredoxin concentrations (see below). With the above corrections for amplitudes, both the calculated (□) and observed (●) spectra should be comparable. As a matter of fact, a very close similarity is found at pH 8. At pH 5.8, the observed spectrum is slightly red-shifted and its maximum is of smaller amplitude compared to the expected spectrum. However its general shape is consistent with its attribution to electron transfer from $(F_A,F_B)^-$ to ferredoxin.

Figure 4 exhibits the decay-associated spectra of the three first-order components observed at pH 8, the sum of which is shown in Figure 3. All three spectra are shown together with the calculated spectrum for electron transfer from F_A,F_B to ferredoxin. For a useful comparison of the spectral shapes, it is essential to plot for each phase the calculated spectrum (□) with an appropriate scaling factor, being equal to the proportion of PSI associated with the corresponding phase. This was done in two steps: (1) first, the same multiplicative factor as defined above was used in order to take into account the proportion of PSI forming a complex with soluble ferredoxin before flash excitation and (2) for each phase, it

Table 1: Properties of Ferredoxin Reduction by PSI

PSI preparation	ferredoxin	experimental conditions	no. of first-order phases: half times	K_d (μM)	second-order rate constant (M^{-1} s^{-1})
monomers/*Sy.* 6803[a]	*Sy.* 6803	pH 8.0, 30 mM NaCl, 5 mM $MgCl_2$	3: 500 ns[b]/13−20 μs/103−123 μs	0.62	$2-5 \times 10^{8}$ [b]
monomers/*Sy.* 6803	*Sy.* 6803	pH 5.8, no salts	2:	0.047	nd[c]
monomers/*Sy.* 6803	spinach	pH 8.0, 30 mM NaCl, 5 mM $MgCl_2$	2: <1 μs/4−6 μs	4−6	5.6×10^{8}
spinach (D144)	*Sy.* 6803	pH 8.0, 30 mM NaCl, 5 mM $MgCl_2$	≥2: <1 μs/>10 μs	≈0.6	nd[c]
spinach (D144)	spinach	pH 8.0, 30 mM NaCl, 5 mM $MgCl_2$	2: <1 μs/4−6 μs	<3	nd[c]

[a] *Synechocystis* sp. PCC 6803. [b] Sétif and Bottin (1994). [c] nd, not determined.

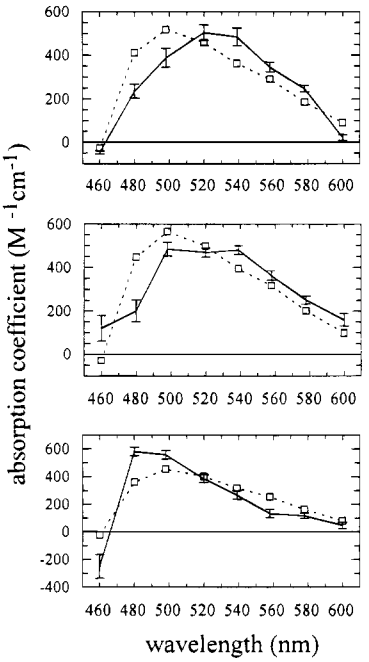

FIGURE 4: Decay-associated spectra of the three components of ferredoxin reduction by monomeric PSI from *Synechocystis* 6803 at pH 8 (—). These spectra result from a global analysis conducted between 460 and 600 nm and correspond to the lower left spectrum of Figure 3 ([PSI] = 0.186 μM, [Fd] = 0.99 μM; see Figure 3 for other experimental conditions). Four different spectra of absorption changes were recorded with samples from the same batch and analyzed independently. The error bars correspond to the extreme values found during the analysis of the four data sets. The upper, middle, and lower spectra correspond respectively to the submicrosecond, 13−20 μs, and 103−123 μs kinetic components. For the sake of comparison, the calculated spectrum for electron transfer from $(F_A,F_B)^-$ to ferredoxin is plotted in each case (□). The amplitude of this spectrum has been calculated in each case from the proportion of PSI−ferredoxin complexes which is associated with the corresponding first-order phase.

was essential to multiply this factor by the proportion of complexed PSI associated with this phase. As the spectra of the three first-order phases are different, these proportions cannot be simply calculated. However it is assumed that a rough estimate can be obtained by integrating the decay-associated spectra of the three first-order components over the 460−600 nm region. Values of 34%, 36%, and 30% were thus found for the proportions of the submicrosecond 13−20 μs, and 103−123 μs phases, respectively.

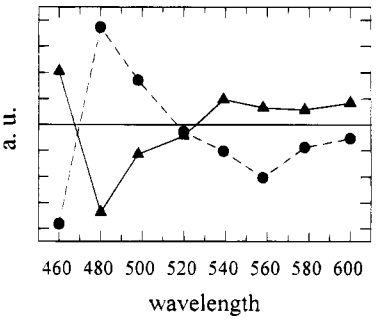

FIGURE 5: Differences between the observed and calculated spectra shown in Figure 4 for the intermediate (13−20 μs; ▲) and slow (103−123 μs; ●) first-order phases.

As previously reported (Sétif & Bottin, 1994), the spectra of the submicrosecond and 13−20 μs phases are rather similar. However a significant difference is observed at 460 nm with some other minor differences at 500 and 600 nm. These spectra were found to be rather similar to the spectra found for the two phases at pH 5.8 (not shown individually; sum shown in Figure 3). The spectrum of the 103−123 μs phase is clearly different from the two preceding spectra in the whole wavelength range, with a blue-shifted maximum, a significant negative amplitude at 460 nm, and some relative decrease in amplitude around 560 nm. However all three spectra are consistent with reduction of ferredoxin by $(F_A,F_B)^-$, although their differences, between them as well as with the calculated spectrum (□), are still to be explained.

It could be informative to put forward more directly the distortions of the decay-associated spectra from the calculated spectrum. Such distortions are plotted in Figure 5 for the intermediate (13−20 μs; ▲) and slow (103−123 μs; ●) first-order phases from the differences between the observed and calculated spectra shown in Figure 4. This was not done for the fast phase as distortions of this phase are of a more complicated origin (see Materials and Methods and Discussion). The spectra of Figure 5 should correspond to distortions of the differential spectra of one or both partners of the electron transfer reaction. These distortions would originate from the interactions between PSI and ferredoxin within the complex and could arise either from F_A,F_B or from ferredoxin (see Materials and Methods). A striking feature of the two plotted spectra is that one is the mirror image of the other. It seems therefore that the spectral distortions due to the PSI−ferredoxin interactions are opposite for the intermediate and slowest first-order phases.

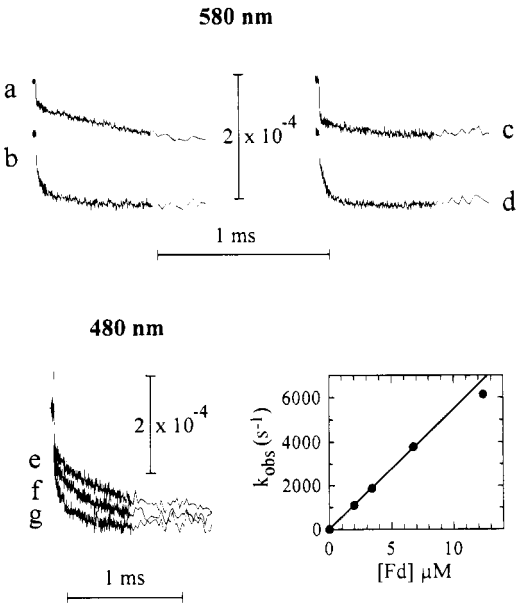

FIGURE 6: Upper part, composite curves measured at 580 nm exhibiting the kinetics of ferredoxin reduction by F_A,F_B. Curve a, 0.203 μM PSI from *Synechocystis* and 2.00 μM spinach ferredoxin; curve b, 0.186 μM PSI and 0.99 μM ferredoxin, both from *Synechocystis*; curve c, 0.157 μM PSI and 1.75 μM ferredoxin, both from spinach; curve d, 0.157 μM spinach PSI and 1.71 μM ferredoxin from *Synechocystis*. Lower part, left, composite curves recorded at 480 nm with PSI from *Synechocystis* (0.186 μM) and variable concentrations of spinach ferredoxin (3.44, 6.76, and 12.4 μM, respectively, for curves e−g). Lower part, right, dependence of the rate of the slower phase observed at 480 nm upon concentration of spinach ferredoxin with PSI from *Synechocystis*. A linear fit of the data for a ferredoxin concentration below 7 μM is also shown (—). It corresponds to k_{obs} (s^{-1}) = [Fd](5.6 × 10^8) M^{-1} s^{-1}. Experimental conditions: 20 mM tricine, pH 8, 30 mM NaCl, 5 mM $MgCl_2$, 10 μM DPIP, 1.5 mM sodium ascorbate, and 0.03% β-DM.

Comparison between Spinach and Synechocystis 6803 at pH 8. In order to detect some possible differences in the rates of ferredoxin reduction in different organisms, we studied reduction of ferredoxin from either spinach or *Synechocystis* by PSI from both origins at pH 8. This is shown in Figure 6 at 580 nm (upper part), where the left and right kinetics were obtained respectively with monomeric PSI from *Synechocystis* and spinach D144 particles. With ferredoxin from *Synechocystis*, the signals recorded with PSI from *Synechocystis* (trace b) and from spinach (trace d) are very similar. Two phases with $t_{1/2}$ < 1 μs and = 13−20 μs are prominent in both cases. With an increased ferredoxin concentration, the signal becomes larger but the same kinetics are observed. Both the submicrosecond and 13−20 μs phases found with spinach PSI are therefore most probably first-order components, as was found with PSI from *Synechocystis*. The presence of a third, slower first-order component was not checked with spinach PSI at 480−500 nm (maximum of amplitude), due to the poor signal to noise ratio of the absorption changes in this wavelength region resulting from the large absorption due to antenna pigments. The sizes of both signals b and d are comparable. When taking into account the concentrations of PSI and ferredoxin for these two curves, it appears that the affinities of *Synechocystis* ferredoxin for both types of PSI are rather similar. When both types of PSI are studied in the presence of spinach ferredoxin (curves a and c), the kinetic profiles are somewhat different from those with ferredoxin from

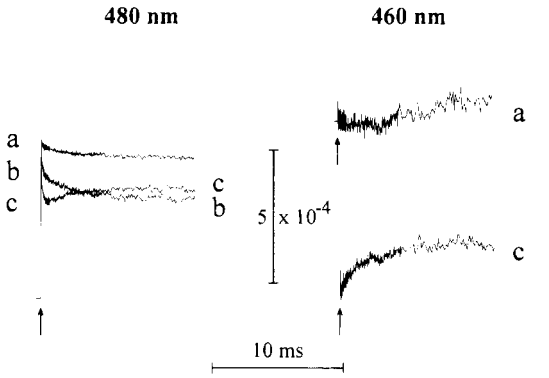

FIGURE 7: Flash-induced absorption changes measured with PSI monomers from *Synechocystis* 6803 at 460 and 480 nm with or without soluble ferredoxin from *Synechocystis*. The PSI reaction centers (0.164 μM) were suspended in 20 mM tricine, pH 8, in the presence of 0.03% β-DM, 30 mM NaCl, 5 mM $MgCl_2$, 1.5 mM sodium ascorbate, and 10 μM DPIP. Curves a, no ferredoxin; curve b, 0.405 μM ferredoxin; curves c, 1.615 μM ferredoxin.

Synechocystis. A major submicrosecond component is clearly visible and followed in both cases by a minor component with $t_{1/2} \approx 4-6$ μs. A more detailed study of ferredoxin reduction by PSI, both prepared from spinach, was not performed. However, comparison of the signal amplitudes of curves a and c suggests that the affinity of spinach ferredoxin is larger for spinach PSI than for PSI from *Synechocystis*. An apparent dissociation constant for spinach ferredoxin and cyanobacterial PSI between 4 and 6 μM can be calculated. The kinetic dependence of ferredoxin reduction upon ferredoxin concentration was further studied with PSI from *Synechocystis* and spinach ferredoxin. This is shown at 480 nm for three different ferredoxin concentrations ([Fd] = 3.44, 6.76, and 12.4 μM for curves e−g). When the ferredoxin concentration is increased, several features of the kinetics emerge (a) both the submicrosecond and 4−6 μs phases are observed in any case, with an increase in amplitude, and (b) a slower phase is present, the rate of which increases and the amplitude of which decreases (making the sum of all three phases of constant amplitude).

The spectra of the three components have been measured (not shown), and they all agree with the process of ferredoxin reduction by F_A,F_B. The rate of the slower component depends linearly on the amount of spinach ferredoxin up to a concentration of 7 μM. This is shown in the right lower part of Figure 6, where only a slight deviation from linearity is observed with a ferredoxin concentration of 12 μM. The second-order rate constant corresponding to this phase is 5.6 × 10^8 M^{-1} s^{-1}. Most of the above results concerning the kinetics of ferredoxin reduction are collected in Table 1.

Evidence for a Fourth Kinetic Phase at High Ferredoxin Concentrations. In the process of ferredoxin reduction by PSI, both from *Synechocystis*, three different first-order phases are found at pH 8 in the presence of salts with $t_{1/2} \approx$ 500 ns and 13−20 and 103−123 μs. In a previous study, it was reported that the kinetic profile is not significantly dependent upon ferredoxin concentration (Sétif & Bottin, 1994). In other words, the relative proportions of the different first-order phases were found to be approximately constant at different ferredoxin concentrations. However the invariability of the kinetics is certainly not true for times longer than 1 ms after flash excitation, as can be seen from Figure 7. This figure exhibits, without any subtraction or

correction procedure, the kinetics observed at 460 and 480 nm on a 12 ms time scale either in the absence of ferredoxin (curves a) or in the presence of ferredoxin at different concentrations (curve b, [Fd] = 0.40 μM; curves c, [Fd] = 1.61 μM). It can be immediately seen that the kinetics of absorption changes recorded at 480 nm are very different for the two ferredoxin concentrations. After the initial fast phases of ferredoxin reduction, a slower decay is observed in curve b. This presumably corresponds to a second-order process of ferredoxin reduction. By contrast, the fast decay observed in curve c is followed by an absorption increase with $t_{1/2} \approx 1.2$ ms. Such an absorption increase is also observed with a larger amplitude at 460 nm (curve c), whereas there is little absorption change at this wavelength in the absence of ferredoxin during 4 ms after flash excitation (curve a). The subsequent slow absorption increase observed at 460 nm in the absence of ferredoxin can be easily interpreted as resulting from the two processes of (a) a recombination reaction between $P700^+$ and $(F_A,F_B)^-$ and (b) a competing process of electron escape from $(F_A,F_B)^-$, at a wavelength where the differences ($P700^+$ − P700) and [$(F_A,F_B)^-$ − F_A,F_B] correspond to opposite absorption changes.

Characteristics of the preceding absorption increase observed in the presence of ferredoxin (hereafter named phase no. 4 as it is the fourth kinetic phase observed with ferredoxin at pH 8 in the order of decreasing rate) are further detailed in Figure 8. Traces c and d were recorded with similar ferredoxin concentrations (1.5−1.7 μM) but with very different PSI concentrations. Ferredoxin is in large excess over PSI for trace c, whereas PSI is in slight excess over ferredoxin for trace d. Comparison of traces c and d reveals that phase no. 4 comes out clearly only in the case where ferredoxin is in excess over PSI. This indicates that the rate of phase no. 4 depends on the concentration of free (oxidized) ferredoxin. Traces a and b were recorded with ferredoxin concentrations of respectively 65 and 11 μM, in both cases in large excess compared to PSI. These two kinetics are very similar, despite the 6-fold difference in ferredoxin concentration. The rate of the absorption increase is plotted versus ferredoxin concentration in the right lower part of Figure 8. It appears that this rate is proportional to the ferredoxin concentration, up to a value of 3 μM, with a second-order rate constant of 3.9×10^8 M^{-1} s^{-1}. It levels off at higher ferredoxin concentrations and reaches an asymptotic value of 2600−2800 s^{-1} ($t_{1/2} \approx 260$ μs). It has to be noted that P700 is not involved in the reaction described above as there is no similar transient observable at 820 nm in the presence of high amounts of ferredoxin (not shown). Trace a is expanded on a shorter time scale in the left lower part of Figure 8. A lag lasting for about 60−100 μs can be seen before the absorption increase develops. Due to this lag, the kinetics at 460 nm were fitted starting from 200 μs after the flash for calculating k_{obs}([Fd]) as shown in Figure 8.

The spectrum of the above process was tentatively measured from 460 to 600 nm. The overall characteristics of this spectrum are small and negative amplitudes from 480 to 600 nm and a larger negative amplitude at 460 nm (an absorption increase corresponding to a negative amplitude of the decay-associated spectrum). It was exhibiting some variations from one sample to another, and further work is still needed before a reliable spectrum can be obtained.

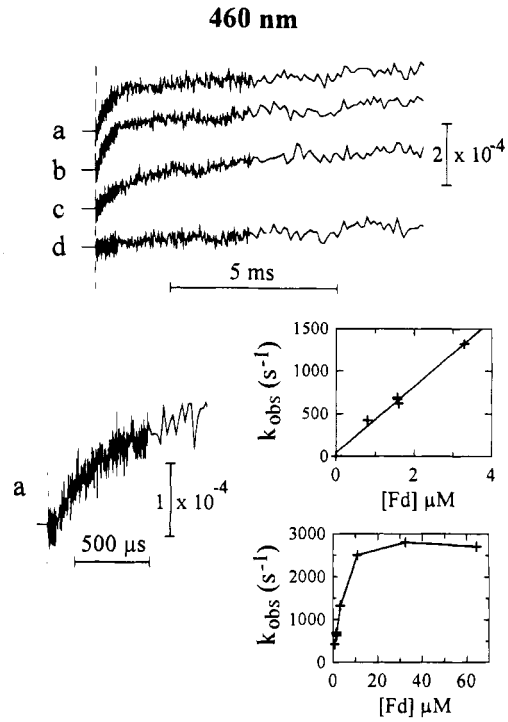

FIGURE 8: Upper part, flash-induced absorption changes measured with PSI monomers from *Synechocystis* 6803 at 460 nm in the presence of variable concentrations of ferredoxin from *Synechocystis*. The time of laser flash excitation is indicated by a dashed line. Curves a, b, and d, 1.7 μM PSI and 1 mm optical pathlength; curve c, 0.17 μM PSI and 1 cm optical pathlength. The ferredoxin concentration is 64.6, 11.0, 1.72, and 1.54 μM for curves a−d, respectively. Curve a is expanded on a shorter time scale in the left lower part. Right lower part, dependence of the rate of the slow phase observed at 460 nm versus ferredoxin concentration (ferredoxin in large excess over PSI). A linear fit is shown for ferredoxin concentrations below 4 μM (upper plot). It corresponds to k_{obs} (s^{-1}) = [Fd](3.9 × 10^8) M^{-1} s^{-1}. Other experimental conditions were as defined in Figure 6.

Nevertheless the above characteristics suggest that it involves partial reoxidation of reduced ferredoxin by some yet unidentified species. However different control experiments indicate that this species is not: (a) dissolved oxygen, as the above reaction is unchanged in the absence of oxygen; depletion of dissolved oxygen was performed in two ways, either with glucose oxidase and catalase in the presence of glucose or by repetitive cycles of freezing and thawing under vacuum; (b) oxidized DPIP, as the same reaction was observed in the absence of added DPIP; these experiments were made using a high concentration of sodium ascorbate (which is a very poor electron donor to $P700^+$ in PSI from *Synechocystis*) and a very low repetition rate of laser flash excitation; (c) dehydroascorbate, as equimolar concentrations of ascorbate and dehydroascorbate did not affect the rate or the size of the observed kinetics. The presence of phase no. 4 was observed with several types of biological materials under the conditions described above (pH 8, 30 mM NaCl and 5 mM $MgCl_2$; fairly large concentration of ferredoxin). (1) With ferredoxin from *Synechocystis* 6803, it was observed using membranes as well as monomeric and trimeric PSI reaction centers from *Synechocystis* and dissolved crystals of PSI trimers from *Synechococcus elongatus* (gift from Dr. P. Fromme, TU, Berlin, Germany). (2) With PSI from *Synechocystis* 6803, it was observed using different ferredoxins besides ferredoxin from *Synechocystis* 6803, such as

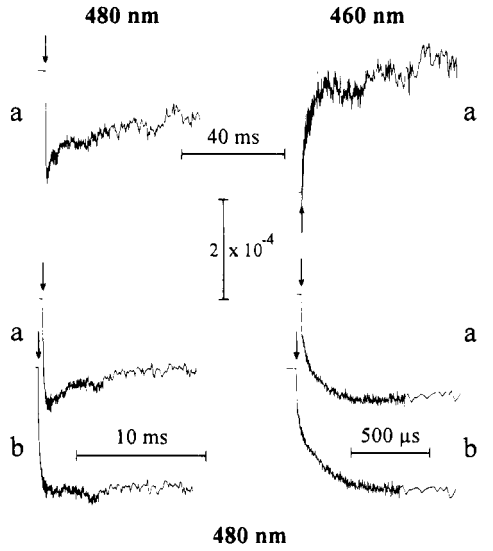

FIGURE 9: Upper part, composite curves measured at 460 and 480 nm at pH 8 (other conditions were as in Figure 7) exhibiting the reduction of soluble ferredoxin and later processes (0.164 μM PSI and 1.615 μM ferredoxin). These composite curves correspond to the data recorded either in the absence or in the presence of ferredoxin that are shown in Figure 7 (traces a and c, respectively). Lower part, all traces correspond to the experiment shown in the upper part at 480 nm. Traces a are expanded parts on shorter time scales. Traces b are derived from traces a after suppression of the absorption changes due to phase no. 4 (see text for details).

ferredoxin from *Spirulina platensis* (Sigma) or from *Chlamydomonas reinhardtii* (gift from Dr. J.-P. Jacquot, University of Orsay, France). Two conditions are reported in this paper where it is not observed, at pH 5.8 in the absence of salts (not shown) or with spinach ferredoxin. In the latter case, this could be due to the fact that phase no. 4 is obscured by the large signal arising from second-order reduction of ferredoxin.

Dependence of the First-Order Kinetics upon Ferredoxin Concentration. Figure 9 shows composite curves (see Materials and Methods) displaying the absorption changes within the PSI acceptors (including ferredoxin) in the presence of ferredoxin on a 70 ms time scale at 460 and 480 nm (traces a of upper part; large excess of ferredoxin compared to PSI). Two slow components are clearly visible on this time scale; the fastest of these two is the reaction described just above (phase no. 4). The $t_{1/2}$ of the slowest component is independent of the ferredoxin concentration and is longer than several 10's of milliseconds. This phase most probably corresponds to slow reoxidation of reduced ferredoxin by dissolved oxygen. Expanded parts of trace a at 480 nm are shown in the lower part of Figure 9 on 12 and 1 ms time scales. In order to study as precisely as possible the first-order kinetics of ferredoxin reduction under such conditions of high ferredoxin concentrations, it appears necessary to eliminate the contribution of phase no. 4 from the absorption changes observed at 480 nm. This cannot be done directly by using a fourth exponential phase, due to the sigmoidal nature of the absorption changes associated with the corresponding process. For an appropriate correction, the following steps were performed. (1) The absorption changes at 460 nm were fitted satisfactorily by two exponential phases; one of these corresponds to phase no. 4, whereas the second one was adjusted in order to fit the lag before development of phase no. 4. (2) Such simulated kinetics were subtracted from the absorption changes ob-

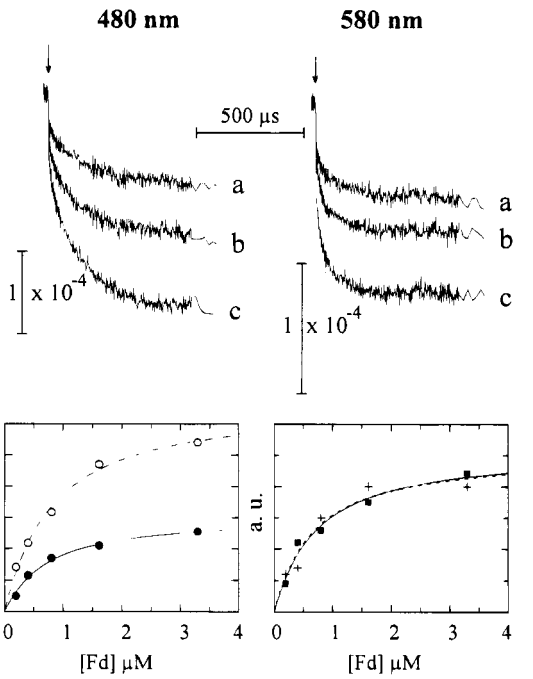

FIGURE 10: Upper part, composite curves measured at 480 and 580 nm. Traces c were corrected for phase no. 4 (see Figure 9 and text for details) and thus should exhibit only the kinetics of ferredoxin reduction by F_A,F_B. The kinetics were recorded at pH 8 (experimental conditions were as in Figure 7) with monomeric PSI and ferredoxin from *Synechocystis* (0.166 μM PSI; the ferredoxin concentration is 0.405, 0.805, and 3.30 μM for curves a–c respectively). Lower part, dependence of the amplitude of different kinetic components on the ferredoxin concentration. A global fit analysis was performed to analyze absorption changes recorded at 480 and 580 nm and at five different ferredoxin concentrations (as those shown in the upper part). Half times of 16 and 117 μs were found from this analysis. The data were fitted assuming a simple binding equilibrium between PSI and ferredoxin, providing an apparent K_d for each of the components. Left, submicrosecond component (●; K_d = 0.62 μM) and 117 μs component (○; K_d = 0.71 μM) at 480 nm. Right, submicrosecond component (■; K_d = 0.62 μM) and 16 μs component (+; K_d = 0.57 μM) at 580 nm.

served at 480 nm with an appropriate multiplicative factor derived from the relative amplitudes of phase no. 4 at 460 and 480 nm. Traces b of Figure 9 were obtained after such corrections to the absorption changes.

From comparison of traces a and b on a 1 ms time scale, it is quite obvious that such a correction is necessary for getting a reliable estimate of the amplitudes of the two components, 13–20 and 103–123 μs, at 480 nm. Such a correction becomes less important at lower ferredoxin concentrations for studying signals on a 1 ms timescale. This is due to the fact that the rate of phase no. 4 decreases at lower ferredoxin concentrations (see Figure 8). As a matter of fact, the data used for the spectral analysis (Figures 3 and 4) were not corrected for phase no. 4, as this phase is much slower ($t_{1/2} \approx 1.7$ ms) than the three first-order phases of ferredoxin reduction with the ferredoxin concentration that was used (0.99 μM). The disturbing presence of phase no. 4 at higher ferredoxin concentrations was also the reason for using only such a small ferredoxin concentration for making the previous spectral analysis, though only 59% of the PSI reaction centers were involved in a preformed PSI–ferredoxin complex (see legend of Figure 3).

Figure 10 (upper part) shows the composite curves exhibiting reduction of ferredoxin at 480 and 580 nm in the

presence of different amounts of ferredoxin (0.405, 0.805, and 3.30 μM respectively for traces a–c), all in excess with respect to PSI. Suppression of the absorption changes due to phase no. 4 was made for ferredoxin concentrations above 1 μM (see above; such corrections are negligible on this time scale for [Fd] < 1 μM). It is observed that, at a given wavelength, the kinetic profiles are almost independent of the ferredoxin concentration. A global analysis with two exponential phases was performed at each ferredoxin concentration for the two kinetics obtained at 480 and 580 nm, thus providing two half times. Each of these two half times exhibits a small variability when repeating the same analysis for five different ferredoxin concentrations ranging from 0.20 to 3.30 μM (deviation from the average value < 15%). This supports the previous conclusion that both components correspond to first-order processes resulting from electron transfer within PSI–ferredoxin complexes that are preformed before flash excitation (Sétif & Bottin, 1994). Furthermore, the similarity of the kinetic profiles, which is observed at a given wavelength, indicates that the proportions of the three different phases are independent of ferredoxin concentration. A global fit analysis with two different exponential phases was then performed for the whole data set (2 wavelengths × 5 ferredoxin concentrations, up to a ferredoxin concentration of 3.30 μM). Half times of 16 and 117 μs were found from this analysis. The amplitudes of the different phases are plotted versus the ferredoxin concentration in the lower part of Figure 10. These data were fitted assuming a simple binding equilibrium between PSI and ferredoxin. Apparent dissociation constants of 0.62 μM were found for the submicrosecond phase at both wavelengths. Dissociation constants of 0.57 and 0.71 μM were calculated for the 16 μs component at 580 nm and the 117 μs component at 480 nm, respectively. The equivalent plots for the 16 μs phase at 480 nm and the 117 μs phase at 580 nm are much less reliable (not shown). Though similar dissociation constants were found, the corresponding data are much more scattered, due to the small relative size of the associated signals (see Figure 4) leading to large relative errors in the estimation of their amplitudes. When the sum of the three components is plotted versus ferredoxin concentration and fitted in the same way as above, apparent dissociation constants of 0.62 μM are found at both 480 and 580 nm.

DISCUSSION

A submicrosecond phase of ferredoxin reduction has been observed in all reactions that we have studied so far. Interestingly, this phase is the dominant first-order process in some cases, e.g., at pH 5.8 with both partners from *Synechocystis* or at pH 8.0 with spinach ferredoxin. This reinforces the previous conclusion (Sétif & Bottin, 1994) that the species reducing ferredoxin (either F_A or F_B) is reduced in less than a few 100's of nanoseconds. With spinach ferredoxin, the presence of a microsecond component of ferredoxin reduction is observed together with the submicrosecond phase. This clearly excludes any large differences in the rates of ferredoxin reduction in *Synechocystis* and spinach, thus casting doubt on the relevance of a previous study reporting rates of ferredoxin reduction (from both spinach and a green alga) around 400 s^{-1} (Hervas et al., 1992). Taking advantage of the relatively low affinity of spinach ferredoxin for *Synechocystis* PSI (K_d = 4–6 μM), it was possible to determine precisely the second-order rate constant of ferredoxin reduction. The observed rate of 5.6 × 10^8 M^{-1} s^{-1} compares well with the second-order rate constant of (2–5) × 10^8 M^{-1} s^{-1} that was found for ferredoxin and PSI, both from *Synechocystis* (Sétif & Bottin, 1994). The two ferredoxins contain five or six basic residues and 20 acidic residues which are located similarly in their highly homologous primary sequences. The similarity in second-order rates would be consistent with a diffusional process that would be primarily determined by the global electrostatic properties of ferredoxin (e.g., the dipole moment), e.g., assuming some kind of guided electrostatic approach of ferredoxin to PSI, as proposed in other systems (Koppenol & Margoliash, 1982; Matthew et al., 1983; De Pascalis et al., 1993).

The existence of three first-order phases of ferredoxin reduction by PSI from *Synechocystis*, with half times of about 500 ns and 20 μs and 100 μs, was previously observed at pH 8 in the presence of salts (Sétif & Bottin, 1994). The slowest of these phases is found to be absent, or at least of a much lower amplitude, in two different kinds of experiments reported here: at pH 5.8 with ferredoxin from *Synechocystis* and with spinach ferredoxin at pH 8. This could suggest that this phase corresponds to a distinct type of PSI–ferredoxin complex. However it is also observed that the absence of the slowest first-order phase is correlated with a larger amplitude of the fastest submicrosecond phase (Figures 3 and 6). This forces us to face the alternative explanation that the fastest and slowest phases could both correspond to a single type of complex, the amplitude of one phase growing at the expense of the other in the frame of a competition process.

A more detailed study of the three phases observed at pH 8 is shown in the present work with monomeric PSI reaction centers from *Synechocystis*. Though fully compatible with the spectrum corresponding to ferredoxin reduction by F_A,F_B that can be independently calculated, the spectra of these three phases exhibit some significant deviations from the calculated spectrum. Despite these deviations, the sum of these three spectra bears a close resemblance, in both shape and amplitude, to the calculated spectrum. The differences in the individual spectra of the three phases together with the close similarity of their sum with the expected spectrum can be tentatively rationalized as follows. The differences between the observed and calculated spectra should arise from distortions of the differential spectra of either F_A,F_B or ferredoxin when the latter is bound to PSI. As shown in Materials and Methods, only distortions due to ferredoxin are involved when considering the sum of all first-order phases. As the spectrum of this sum resembles closely the calculated spectrum, two explanations can be proposed for such a similarity: (1) The distortions (due to ferredoxin) in the different types of complexes are significant but fortuitously cancel each other [$(1 - \alpha - \beta)V_I + \alpha V_{II} + \beta V_{III} \approx 0$; see Materials and Methods], which appears unlikely but cannot be excluded. (2) These distortions are negligible, i.e., each term of the preceding sum (V_I, V_{II}, and V_{III}) is of small amplitude. We favor this last explanation for the results obtained at pH 8. However, the same line of reasoning cannot be sustained for the results obtained at pH 5.8, as the spectrum of the sum of the first-order components significantly deviates from the calculated spectrum (Figure 3, lower right). This could originate from the fact that the individual difference spectra of F_A,F_B and ferredoxin, which

were used for deriving the calculated spectrum, were measured at pH's 8 and 8.5, respectively. Alternatively, the 2Fe-2S cluster of ferredoxin could be slightly distorted at pH 5.8 when ferredoxin is bound to PSI, thus leading to some spectral changes. The latter possibility would be in line with the much larger affinity of ferredoxin for PSI that is observed at pH 5.8 ($K_d \approx 0.05$ μM) compared to at pH 8. With regard to the fast (submicrosecond) phase, it appears that deviation of its spectrum from the calculated spectrum can have several origins, being due either to ferredoxin involved in the fast phase or to F_A,F_B involved in the two slower components (see Materials and Methods). This results from the procedure used for studying the ferredoxin reduction process, which makes use of a difference between absorption changes observed in the presence and absence of ferredoxin.

It is observed that deviations from the calculated spectrum are opposite when considering the spectra that are observed at pH 8 for the intermediate phase on the one hand and for the slowest phase on the other hand (Figure 5). Assuming, as discussed above, that distortions due to ferredoxin are of small amplitude at pH 8 (V_{II} and $V_{III} \approx 0$), it follows that distortions due to F_A,F_B should be approximately opposite ($U_{II} \approx -U_{III}$) when considering these two phases. This can be explained by assuming that these two phases correspond to two different binding sites of PSI for ferredoxin. It also strongly suggests that these two sites are geometrically distinct as a slight rearrangement of ferredoxin relative to PSI in one site versus the other is not expected to lead to opposite spectral modifications. We further speculate that the partner of ferredoxin differs in these two sites (F_A in one site and F_B in the other), as differences in the spectra of (F_A^- − F_A) and (F_B^- − F_B) can receive the two following types of explanations.

(1) The spectra of the differences (F_A^- − F_A) and (F_B^- − F_B) can be intrinsically different. When one measures the differential spectrum corresponding to the one-electron reduction of F_A,F_B, the reduced state probably corresponds to an equilibrium between the two redox states F_A^-,F_B and F_A,F_B^-, as this equilibrium should be much faster than electron transfer to methylviologen ($t_{1/2} > 1$ ms). This can be inferred from the small center to center distance between F_A and F_B ($d = 12$ Å; Krauss et al., 1993) and from NMR studies of bacterial 8Fe-8S ferredoxins, similar to subunit PSI-C of PSI carrying both F_A and F_B, which have shown that electron transfer between the two 4Fe-4S centers occurs with $t_{1/2} < 10$ μs (Bertini et al., 1992).

(2) The spectra of (F_A^- − F_A) and (F_B^- − F_B) are different only in the presence of ferredoxin. Such a difference could arise from electrochromic shifts [see, e.g., Witt 1979)] due to the large number of negative charges surrounding the 2Fe-2S cluster of ferredoxin and most probably facing the PSI binding site. With such an explanation, the electrochromic shifts should be in opposite directions for the two sites considered above, in order to explain the experimental observations. Many electronic transitions are involved in the absorption of iron−sulfur centers in the visible region. Several requirements must be met for the observations of such large (≈20 nm) electrochromic shifts in opposite directions. First, there must exist a difference in the permanent dipoles of the ground and excited states (respectively μ_g and μ_e) that are involved in the transitions. This must be the case for either the oxidized form of the iron−sulfur center, the reduced form, or both. Second, for the effects to be opposite on F_A and F_B, one has to assume that the electric field induced by bound ferredoxin is of roughly opposite direction for the two sites with regard to the orientation of ($\mu_g - \mu_e$). Third, one has to assume that these effects, if effective on a single transition of a given redox state of one iron−sulfur center, will not average to zero when considering, at a given wavelength, the contributions of all transitions on the differential (oxidized minus reduced) absorption spectra. That these three conditions are met certainly needs to be confirmed, which may be a huge task but is an open possibility.

In line with the above discussion and whichever precise explanation for the observed spectral difference is correct, we will assume in the following the existence of two well-separated sites, I and II. The existence of two different sites has been recently proposed from the X-ray structure of PSI at a 6 Å resolution (Fromme et al., 1994). A docking site was proposed for ferredoxin with a 14 Å center to center distance between F_{II} (either F_A or F_B, the farthermost from the stromal surface) and the 2Fe-2S cluster of ferredoxin. Another site was speculated, approximately at the opposite site of the PSI stromal hump, for which ferredoxin is much closer to F_I (the closest to the stromal surface) than to F_{II}, with a 19 Å center to center distance between the iron−sulfur clusters. We further speculate that these two sites would be associated with electron transfer from F_I and F_{II}, respectively.

The three first-order phases that are observed at pH 8 with PSI and ferredoxin from *Synechocystis* 6803 are followed by another kinetic component which is most clearly visible at 460 nm and was mentioned before as phase no. 4. The following points suggest that this phase corresponds to some partial reoxidation of reduced ferredoxin by some yet unknown species, which is triggered by some collisional processes involving free ferredoxin.

A lag of 60−100 μs duration is present before the appearance of phase no. 4 (Figure 8). This can be easily explained if the lag corresponds to the time needed for ferredoxin reduction. That the lag duration approximately corresponds to the slowest first-order phase could imply that only ferredoxin reduced through this phase gives rise to the reoxidation monitored by phase no. 4. However, it is quite possible that some other step is rate-limiting for such a reoxidation (e.g., the rate of ferredoxin dissociation from PSI).

A linear relationship is found between the rate of phase no. 4 and the concentration of free ferredoxin when lower than 4 μM (Figure 8). The corresponding second-order rate constant is about 4×10^8 M^{-1} s^{-1} which is close to the value found for the second-order rate constant of ferredoxin reduction [$(3-5) \times 10^8$ M^{-1} s^{-1}; Sétif & Bottin, 1994]. This suggests that the same collisional process is involved in both cases, which in turn implies that the rate constant of this process is not significantly influenced by ferredoxin being already bound to PSI.

It is observed that the rate of phase no. 4 reaches an asymptotic value of about 2600−2800 s^{-1} ($t_{1/2} \approx 260$ μs) at high ferredoxin concentrations. This indicates that another rate-limiting reaction is involved in this process. Though several of its characteristics have been determined, the exact nature of the reaction(s) giving rise to phase no. 4 is still not clear and is the subject of further investigation. However, it has been necessary to eliminate its contribution for studying

with a greater accuracy the different first-order phases of ferredoxin reduction at pH 8. This is particularly true when using relatively high concentrations of ferredoxin for which phase no. 4 contribution interferes considerably with the slowest first-order component. After such corrections, it is possible to study much more reliably the dependence of the kinetics of ferredoxin reduction by PSI on the ferredoxin concentration. From this study, performed at 480 and 580 nm (Figure 10), it appears that the relative proportions of the three reduction phases do not depend upon ferredoxin concentration, up to 3.3 μM. As at least two different types of complexes are present, this implies that these complexes are mutually exclusive or at least that there is significant anticooperativity in ferredoxin binding to PSI. In the opposite case where two ferredoxins could be bound to one PSI complex, the kinetics of ferredoxin reduction are expected to depend strongly on the ferredoxin concentration, assuming a competition process for reduction at the different sites. As shown in Materials and Methods for the case of mutually exclusive complexes, the apparent dissociation constant that can be calculated assuming a simple binding equilibrium between PSI and ferredoxin (0.62 μM at pH 8) is

$$K = 1/[\sum_{(i=1..n)} (1/K_{d_i})]$$

(summation over all types of complex), with K_{d_i} being the dissociation constant of complex no. *i*.

The dissociation constant K_{d_i} is identical to the ratio of K over the proportion of PSI involved in complex no. *i* compared to the total PSI complexed to ferredoxin (see Materials and Methods). These proportions can be approximated by integrating the decay-associated spectra of the three first-order components over the 460−600 nm region (see Results). Proportions of 34%, 36%, and 30% were thus found for the submicrosecond, 13−20 μs, and 103−123 μs phases, respectively. Assuming three different types of complexes leads to dissociation constants of 1.82, 1.68, and 2.07 μM for the above three components. If two of these three phases are associated to a single type of complex, the corresponding dissociation constant can be easily calculated from the above numbers.

ACKNOWLEDGMENT

We thank Dr. J.-P. Jacquot for providing us with spinach ferredoxin.

REFERENCES

Andersen, B., Koch, B., & Scheller, H. V. (1992a) *Physiol. Plant. 84*, 154−161.
Andersen, B., Scheller, H. V., & Møller, L. (1992b) *FEBS Lett. 311*, 169−173.
Arnon, D. I. (1949) *Plant Physiol. 24*, 1−15.
Beechem, J. M. (1992) *Methods Enzymol. 210*, 37−54.
Bertini, I., Briganti, F., Luchinat, C., Messori, L., Monnanni, R., Scozzafava, A., & Vallini, G. (1992) *Eur. J. Biochem. 204*, 831−839.
Boardman, N. K. (1971) *Methods Enzymol. 23* (A), 268−276.
Bottin, H., & Lagoutte, B. (1992) *Biochim. Biophys. Acta 1101*, 48−56.
De Pascalis, A. R., Jelesarov, I., Ackermann, F., Koppenol, W. H., Hirasawa, M., Knaff, D. B., & Bosshard, H. R. (1993) *Protein Sci. 2*, 1126−1135.
Fee, J. A., & Palmer, G. (1971) *Biochim. Biophys. Acta 245*, 175−195.
Fromme, P., Schubert, W.-D., & Krauss, N. (1994) *Biochim. Biophys. Acta 1187*, 99−105.
Golbeck, J. H., & Bryant, D. A. (1991) in *Current Topics in Bioenergetics* (Govindjee, Ed.) pp 83−177, Academic Press, London.
Hervas, M., Navarro, J. A., & Tollin, G. (1992) *Photochem. Photobiol. 56*, 319−324.
Ho, K. K., & Krogmann, D. W. (1984) *Biochim. Biophys. Acta 766*, 310−316.
Ke, B. (1973) *Biochim. Biophys. Acta 301*, 1−33.
Koppenol, W. H., & Margoliash, E. (1982) *J. Biol. Chem. 257*, 4426−4437.
Krauss, N., Hinrichs, W., Witt, I., Fromme, P., Pritzkow, W., Dauter, Z., Betzel, C., Wilson, K. S., Witt, H. T., & Saenger, W. (1993) *Nature 361*, 326−330.
Kruip, J., Boekema, E. J., Bald, D., Boonstra, A. F., & Rögner, M. (1993) *J. Biol. Chem. 268*, 23353−23360.
Lelong, C., Sétif, P., Lagoutte, B., & Bottin, H. (1994) *J. Biol. Chem. 269*, 10034−10039.
Mathis, P., & Sétif, P. (1981) *Isr. J. Chem. 21*, 316−320.
Matthew, J. B., Weber, P. C., Salemme, F. R., & Richards, F. M. (1983) *Nature 301*, 169−171.
Rogers, L. J. (1987) in *The Cyanobacteria* (Fay, P., & Van Baalen, C., Eds.), pp 35−67, Elsevier, Amsterdam.
Rögner, M., Nixon, P. J., & Diner, B. A. (1990) *J. Biol. Chem. 265*, 6189−6196.
Rousseau, F., Sétif, P., & Lagoutte, B. (1993) *EMBO J. 12*, 1755−1765.
Sétif, P., & Bottin, H. (1994) *Biochemistry 33*, 8495−8504.
Sonoike, K., Hatanaka, H., & Satoh, S. (1993) *Biochim. Biophys. Acta 1141*, 52−57.
Tagawa, K., & Arnon, D. I. (1968) *Biochim. Biophys. Acta 153*, 602−613.
Witt, H. T. (1979) *Biochim. Biophys. Acta 505*, 355−427.
Zanetti, G., & Merati, G. (1987) *Eur. J. Biochem. 169*, 143−146.
Zilber, A. L., & Malkin, R. (1988) *Plant Physiol. 88*, 810−814.

BI950479L